Chinese Chemical Letters 31 (2020) 10–18

Contents lists available at ScienceDirect

Chinese Chemical Letters

journal homepage: www.elsevier.com/locate/cclet

Review

Advances in self-assembly and regulation of aromatic carboxylic acid derivatives at HOPG interface

Jianqiao Li[a,b,d], Xiaoyi Zu[a,b], Yuxin Qian[a,b], Wubiao Duan[a,*], Xunwen Xiao[d,*], Qingdao Zeng[b,c,*]

[a] Department of Chemistry, School of Science, Beijing Jiaotong University, Beijing 100044, China
[b] CAS Key Laboratory of Standardization and Measurement for Nanotechnology, CAS Center for Excellence in Nanoscience, National Center for Nanoscience and Technology (NCNST), Beijing 100190, China
[c] Center of Materials Science and Optoelectonics Engineering, University of Chinese Academy of Sciences, Beijing 100049, China
[d] College of Chemical Engineering, Ningbo University of Technology, Ningbo 315211, China

ARTICLE INFO

Article history:
Received 14 January 2019
Received in revised form 26 March 2019
Accepted 15 April 2019
Available online 17 April 2019

Keywords:
Aromatic carboxylic acid
Self-assembly
Molecular templates
Host-guest systems
Photo-isomerization
Scanning tunneling microscopy (STM)

ABSTRACT

Aromatic carboxylic acid self-assembly has been a hot research field for many scientists due to its strong coordination ability and flexible coordination mode. The hydrogen bond formed between aromatic carboxylic acids is a strong intermolecular force and has directionality and saturation, which plays a very important role in the self-assembly and regulation of aromatic carboxylic acids. In this review, we introduce surface organization formed by aromatic carboxylic acids with the aid of scanning tunneling microscopy (STM). These two-dimensional structures include molecular templates, host-guest systems, and photo-isomerization structures. We also emphasize the thermodynamics and dynamics, which are important research topics of current and future study.

© 2019 Chinese Chemical Society and Institute of Materia Medica, Chinese Academy of Medical Sciences. Published by Elsevier B.V. All rights reserved.

1. Introduction

One of the current focuses of two-dimensional (2D) supramolecular chemistry is to control the spatial organization of the chemical functions of surfaces at the molecular scale [1–6], for example, the structure changes with external environments like concentration [7–10], temperature [11], light and voltage [12–15], entrapping and releasing guest molecules by regulating the host grids [16–23] and so forth. Molecular self-assembly through non-covalent interactions is one of the main processes to form supramolecular arrays. These molecular layers can be self-assembled on a variety of surfaces, such as highly ordered pyrolytic graphite (HOPG), mica, gold, copper, silicon [24]. Non-covalent interactions include hydrogen bonds [25–27], van der Waals force [28–30], π-π interactions [31–33] electrostatic force [34,35]. It is worth noting that hydrogen bonds own excellent characteristics of intermolecular interactions. Due to their strength, selectivity and directionality, the assemblies of hydrogen-bonded networks have advantages of predictable shapes, easy synthesis as well as reversible dynamic behavior, which can optimize their performance in different situations [36–41].

Aromatic carboxylic acids have strong coordination ability and flexible coordination mode [42–44]. The aromatic ring in the aromatic carboxylic acid ligand has a conjugated system which is favorable for electron transfer, and the carboxyl oxygen atom can form hydrogen with the solvent molecule. Therefore, the aromatic carboxylic acid has the ability to form a stable supramolecular structure and exhibits novel and unique physicochemical properties. Aromatic carboxylic acid self-assembly has been a hot research field for many scientists [45–53].

Scanning tunneling microscopy (STM) has become a useful tool of choice for characterizing 2D nanostructured arrays [54–60]. STM provides direct visual cues for molecular organization on solid-gas interfaces, solid-liquid interfaces or in ambient environments. The principle of STM is to measure the electric current through the tip and substrate as a function of spatial position, and the data obtained includes information about the topography and electronic structures. Thus, the STM tips can also be used as an effective tool for local stimuli to execute surface reactions [61–63]. In a word, STM technology has great application potential, such as monitoring molecular dynamics, substrate-induced recombination, molecular manipulation and surface chirality [64–70].

* Corresponding authors.
E-mail addresses: wbduan@bjtu.edu.cn (W. Duan), xunwenxiao@nbut.edu.cn (X. Xiao), zengqd@nanoctr.cn (Q. Zeng).

https://doi.org/10.1016/j.cclet.2019.04.032
1001-8417/© 2019 Chinese Chemical Society and Institute of Materia Medica, Chinese Academy of Medical Sciences. Published by Elsevier B.V. All rights reserved.

In this review, we focus on surface organization of hydrogen bonds formed by aromatic carboxylic acids. The hydrogen bonding ability has been effectively utilized to achieve the desired morphology and nanostructure on the HOPG surface under ambient conditions. In addition, the host-guest system is also investigated by introducing guest molecules into a template formed by hydrogen bonds. All kinds of molecules used in the review are shown in Scheme 1.

2. Molecular templates on HOPG surface

C3-symmetric π-conjugated planar molecules (Tp, T12, T18, and Ex) are self-assembled at the HA/HOPG interface [71,72]. These molecules have similar structural central cores but their side lengths are different. In the case of Tp molecules, the self-assembled structure of these flower-shaped molecules is show in Fig. 1a. Each Tp molecule links six adjacent molecules to form large-scale networks. Two triangle-like cavities of the networks are observed in Fig. 1b. The small cavity, called the PhT motif, consists of three peripheral 4,4′-dicarboxy-*o*-terphenyl groups, as shown in Fig. 1c the grayscale part. The larger triangle cavity consists of six benzoic acid groups from six peripheral 4,4′-dicarboxy-*o*-terphenyl groups (Fig. 1c). The clover-shaped molecules T12 assemble into equilateral-triangle-like domains with sizes of a few tens of nanometers, as shown in Fig. 1d. This is because the solvent HA molecules interact with T12 at the boundary between the domains. Similar to Tp, each T12 molecule connects with six adjacent molecules and two kinds of cavities are observed in one domain (Fig. 1e). Due to the similar PhT motif, the small triangular cavity is approximately equal to the triangular cavity of Tp. The calculated molecular model shows that the irregular hexagonal-shaped cavity consists of six benzoic acid groups from six peripheral 4,4′-dicarboxy-*o*-terphenyl groups and three sides of the central core from three T12 molecules (Figs. 1f-h). The self-assemblies of T18 and Ex have analogous porous arrangements. Molecules of T18 self-assemble into two kinds of cavities, PhT motifs and hexagonal-shaped cavity (Figs. 1i and j). According to the molecular structure, there should be a third cavity in the middle of the T18 (Fig. 1k). However, the cavity could not be observed from the STM results. Ex networks are similar to T18 networks, but with larger triangular cavities, and the third triangular cavity in the middle of the molecule Ex can be observed (Figs. 1l and n). As the molecular size increases, the thermal stability of the four molecular components gradually decreases calculated by DFT method. The investigation of these molecules' self-assembled structures provides important guidance in the design of functional conjugated molecules for specific applications [73].

HPB-based compounds are highly symmetrical molecules that can exhibit a particular arrangement that is replaced by an interactive group [74–77]. A series of hexaphenylbenzene (HPB) derivatives (HPB-1,3,5-3 A, HPB-1,2,4-3 A, and HPB-1,4-2 A) have been self-assembled at both 1-phenyloctane/HOPG and HA/HOPG interfaces. These molecules are substituted with different numbers of carboxyl groups at different positions. HPB-1,3,5-3 A molecules self-assemble at the PO/HOPG interface as shown in Fig. 2a. Mainly four types of cavities are formed, including pentagon, hexagon, heptagon, and octagon structures (Fig. 2b). Pentagonal, hexagonal, heptagonal and octagonal rings are formed and hexagonal rings are the most common. Three rings connected with a common vertex can be denoted as the "6-6-6" circle "7-5-6" circle and "8-5-6" circle. The 6-6-6 system is more stable than the 7-5-6 and 8-5-6 systems calculated by DFT method. Asymmetrical molecule HPB-1,2,4-3 A assembles into four locally ordered patterns at the PO/HOPG interface (Figs. 2d and e). HPB-

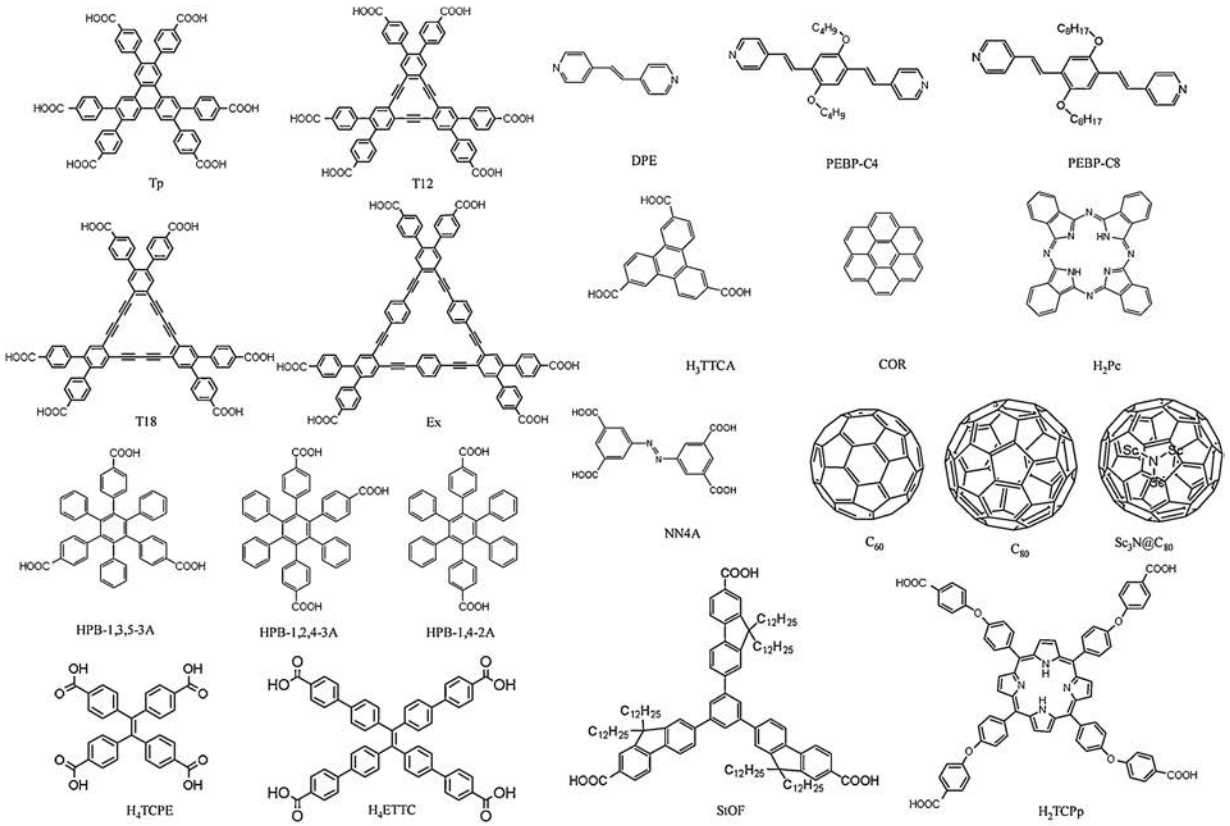

Scheme 1. Molecular structures involved in self-assembly in the review.

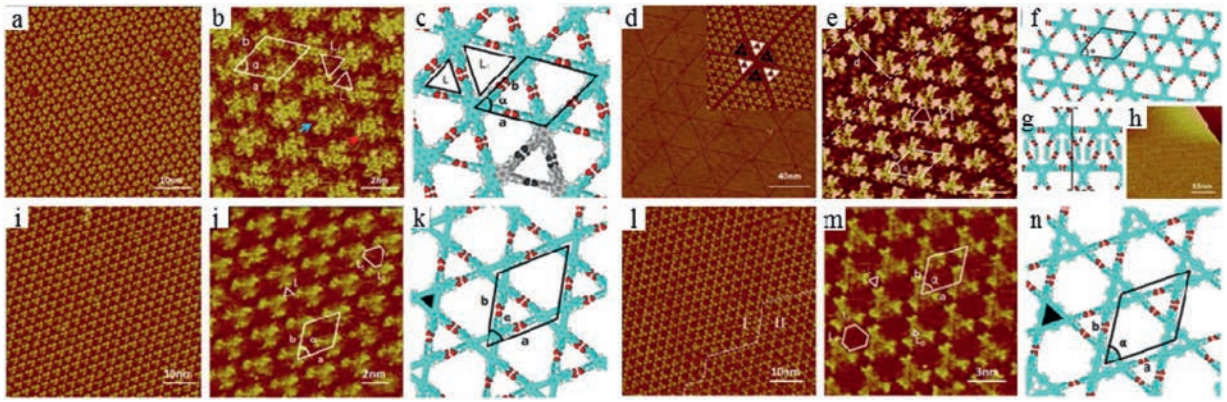

Fig. 1. (a) Large-scale and (b) high-resolution STM images of the assembled structure of Tp at the 1-heptanoic acid (HA)/HOPG interface. (c) Calculated molecular models for the assembled structure of Tp. (d) Large-scale and (e) high-resolution STM images of the assembled structure of T12 at the HA/HOPG. (f) High-resolution STM image of the assembled structure of T12 at the HA/HOPG interface. Calculated molecular models for the assembled structures of T12 (f) and T12-HA (g). (h) Large-scale STM image of the assembled structure of T12 at the 1-phenyloctane/HOPG interface. (i) Large-scale and (j) high-resolution STM images of the assembled structure of T18 at the HA/HOPG interface. (k) Calculated molecular models for the assembled structure of T18. (l) Large-scale and (m) high-resolution STM imaged of the assembled structure of Ex at the HA/HOPG interface. (n) Calculated molecular models for the assembled structure of Ex. Reproduced with permission [73]. Copyright 2017, Wiley-VCH Verlag GmbH & Co. KGaA.

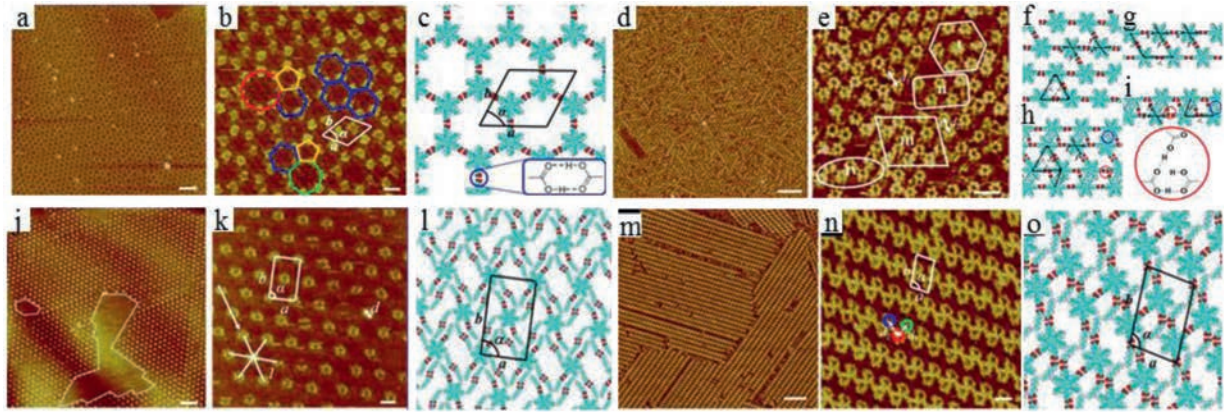

Fig. 2. (a) Large-scale STM image of HPB-1,3,5-3 A monolayers at the PO/HOPG interface. (b) High-resolution STM image of HPB-1,3,5-3 A self-assembled structure. (c) Suggested molecular model for the structure marked with blue hexagons. (d) Large-scale STM image of HPB-1,2,4-3 A monolayers at the PO/HOPG interface. (e) High-resolution STM image corresponding to image (d). (f–i) Molecular models of domains I, II, III and IV. (j) Large-scale STM image of HPB-1,4-2 A monolayers at the HA/HOPG. (k) High-resolution STM image of HPB-1,4-2 A assembled Structure. (l) Suggested structure model of HPB-1,4-2 A self-assembly on HOPG surface. (m) Large-scale STM image of HPB-1,2,4-3 A monolayers at HA/HOPG interface. (n) High-resolution STM image of HPB-1,2,4-3 A self-assembled structure. (o) Suggested molecular model for HPB-1,2,4-3 A architecture in STM image (n). Reproduced with permission [78]. Copyright 2016, American Chemical Society.

1,2,4-3 A molecules are joined along the *para*-substituted (1, 4) carboxylic acid to form molecular wires. The orientation of the other substituent determines the formation of a grid or linear structure. The molecular models for these structures show the arrangement clearly (Figs. 2f-h). The HPB-1,4-2 A molecules cannot obtain self-assembled structures at PO/HOPG interface but they can be loosely arranged by bridging the HA molecules (Fig. 2j). The solvent HA interacts with carboxylic acid groups of the HPB-1,4-2 A molecules through hydrogen bonds and these HPB-1,4-2 A molecules are aligned into cavities (Fig. 2h). HPB-1,2,4-3 A molecules self-assemble into a well-ordered lamellar structure at the HA/HOPG interface (Fig. 2m). Each of the two HPB-1,2,4-3 A molecules interacts through a hydrogen bond between one of the three carboxyl groups and forms a dimer in the shape of a bowknot. The solvent HA molecule interacts with the other two carboxyl groups of the HPB-1,2,4-3 A molecule by hydrogen bonding and is arranged in parallel with the alkyl chain of the HA molecule of the HPB-1,2,4-3 A bridge (Fig. 2n). The lamellar structures composed of bowknot-shaped dimers are formed by van der Waals interactions [78].

3. Host-guest structures on HOPG surface

The host-guest system of self-assembled structures has been investigated [79–82]. Triphenylene-2,6,10-tricarboxylic acid (H_3TTCA) can be regarded as a central triphenylene with a threefold symmetric carboxylic acid functionality. At the HA/HOPG interface, H_3TTCA molecules exclusively self-assemble into honeycomb networks *via* intermolecular hydrogen bonds between carboxyl groups (Fig. 3a). COR molecules are chosen as the guest molecules to hybridize with H_3TTCA. There are three patterns of H_3TTCA/COR co-adsorption structures, denoted as the domain I, II and III. Concentration experiments are carried out to reveal the formation mechanism of each pattern. The H_3TTCA/COR(I) pattern the domain is observed at a low concentration of COR solution (Fig. 3c). The H_3TTCA host honeycomb network has been broken down into separate hexagonal rings. One COR molecule is strongly entrapped into the triangle-like cavity formed by three vacant H_3TTCA hexagonal rings. By increasing the concentration of the COR solution, H_3TTCA/COR(II) pattern is obtained (Fig. 3e). In this pattern, the original vacant hexagonal cavities in the domain I are

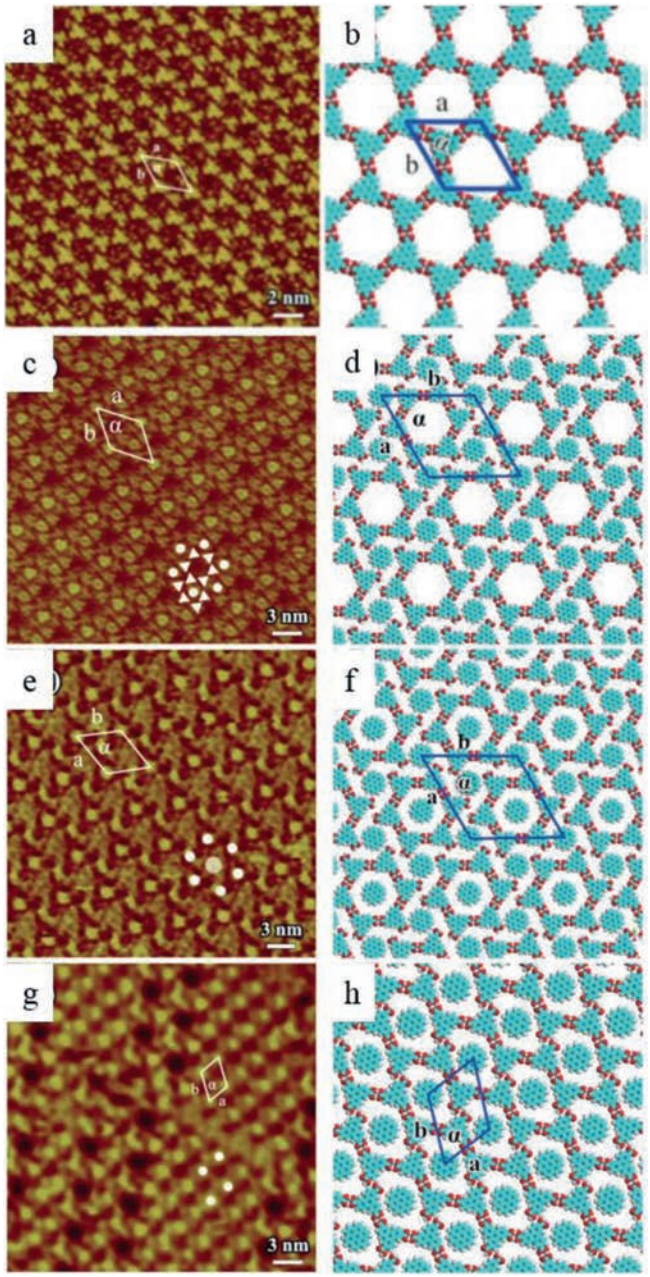

Fig. 3. (a) A high resolution STM image of the self-assembled structure of H_3TTCA networks on the HOPG. (b) The proposed molecular model for H_3TTCA. The high resolution (c) STM image and the molecular model (d) of H_3TTCA/COR(I) at 10% saturation of COR. The high resolution STM image (e) and the molecular model (f) of H_3TTCA/COR(II) at 50% saturation of COR. The high resolution (g) STM image and the molecular model (h) of H_3TTCA/COR(III) at 100% saturation of COR. Reproduced with permission [83]. Copyright 2015, The Royal Society of Chemistry.

filled by COR molecules. The COR can rotate and move slightly inside the pore since the pore is too large for the COR. With an increase of the COR concentration, linear structures (pattern H_3TTCA/COR(III)) gradually appear (Fig. 3g). During the process, more H-bonds are broken and the honeycomb network is transformed to parallel quadrilateral cells. The COR molecules are linearly captured into the cavities at a higher molecular packing density. It is inferred that spatial matching and concentration-dependent effects play an important role in the transformation of H_3TTCA host network structures after introducing the COR guest molecule. DFT calculations of the three structures reveal that the stability of the H_3TTCA/COR structures gradually decreases as the concentration of COR increases, which means the host-guest structural polymorphism is most associated with the solution concentration [83].

Unlike the COR molecule mentioned before, H_2Pc is a two-fold symmetrical molecule and it is geometrically mismatched with H_3TTCA pores. After inserting H_2Pc molecules, the original chicken-wire structures rearrange into zigzag molecular rows along one direction. Five kinds of molecular nanoarrays of H_2Pc embed into the H_3TTCA arrays. $2H_2$Pc@H_3TTCA is composed of one H_2Pc-formed dimer and two H_3TTCA (Fig. 4a); $3H_2$Pc@H_3TTCA consists of a trimer of H_2Pc and two H_3TTCA (Fig. 4b); $4H_2$Pc-zigzag@H_3TTCA is composed of a zigzag-shaped tetramer of H_2Pc and two H_3TTCA (Fig. 4c); the composition of $5H_2$Pc-zigzag@H_3TTCA (Fig. 4d) is a linear and $5H_2$Pc-line@H_3TTCA (Fig. 4e) or a zigzag array of the H_2Pc pentamer and two H_3TTCA respectively. The H_2Pc arrays interact with each other through van der Waals and can be stabilized only by interaction with weak hydrogen bonds of H_3TTCA and H_3TTCA dimers in one direction. $2H_2$Pc@H_3TTCA is proved to be the most stable array of the five nanoarrays by DFT calculations. Then, changing the temperature is an approach to getting the most stable structure [84,85]. After annealing the samples, the nanoarrays discussed above precisely change into close-packed arrays of the $2H_2$Pc@H_3TTCA structure (Fig. 4f). The nH_2Pc@H_3TTCA structures give us the insight into dynamic procedures of self-assembly and control molecular pattern formation on the surface [86].

Tetraphenylethylene (TPE) and its derivatives (H_4TCPE and H_4ETTC) have great potential in such applications as biological and chemical sensors [87–89] and optoelectronic materials [90–94]. The H_4TCPE molecules formed well-aligned lamellar structures at the HA/HOPG interface, co-assembled with HA *via* hydrogen bonds (Fig. 5a). Due to the spatial characteristics of the propeller structure, all of the phenyl groups of the H_4TCPE molecule remain perpendicular to the HOPG surface and interact with the substrate *via* edge-to-face π-π interaction. While H_4ETTC molecules are observed as bigger X-shaped molecules and self-assemble into quadrilateral structures (Fig. 5c). To further investigate the self-assembly behaviors of H_4TCPE and H_4ETTC, three kinds of pyridine derivatives (DPE, PEBP-C4 and PEBP-C8) are introduced into their self-assembled structures separately. After diluting the solution of DPE, there is non-transformation of the H_4TCPE structure. This can be attributed to the high hydrogen bond density and the lack of spatial chemical structure. H_4ETTC/DPE can co-assemble into two lamellar structures at different proportion of DPE molecules in the system. At a saturated concentration of DPE, H_4ETTC and DPE self-assemble into a closely packed lamellar structure (Fig. 5e). By increasing the content of DPE twice, a loosely packed lamellar structure is constructed (Fig. 5g). DPE molecules assemble into dimers and O—H···O interactions between H_4ETTC molecules are completely broken. DFT results that with the addition of different contents of DPE, the loosely packed structure of H4ETTC/DPE is much more stable than the closely packed structure. With the introduction of PEBP-C4 solution, only a few H_4TCPE and PEBP-C4 can co-assemble (Fig. 5i, marked by red rectangles), The H_4TCPE molecules are arranged in a row and distributed between the PEBP-C4 molecules. H_4ETTC/PEBP-C4 assembled structures are shown in Fig. 5k. In the well-ordered lamellar acid-pyridine-acid-pyridine structures, PEBP-C4 molecules interact with the HA solution molecules through O—H···N hydrogen bonds, and these HA molecules are linked to the H_4ETTC molecule through the O—H···O interaction. Similar to the H_4TCPE assembly to PEBP-C4, only a few co-assembled structures (Fig. 5m, labeled by red rectangles) are co-adsorbed after introducing PEBP-C8. In H_4TCPE/PEBP-C8 system, all of the phenyl groups of H_4TCPE remain perpendicular to the substrate, two of which are linked to the HA and PEBP-C8 molecules by O—H···O and O—H···N

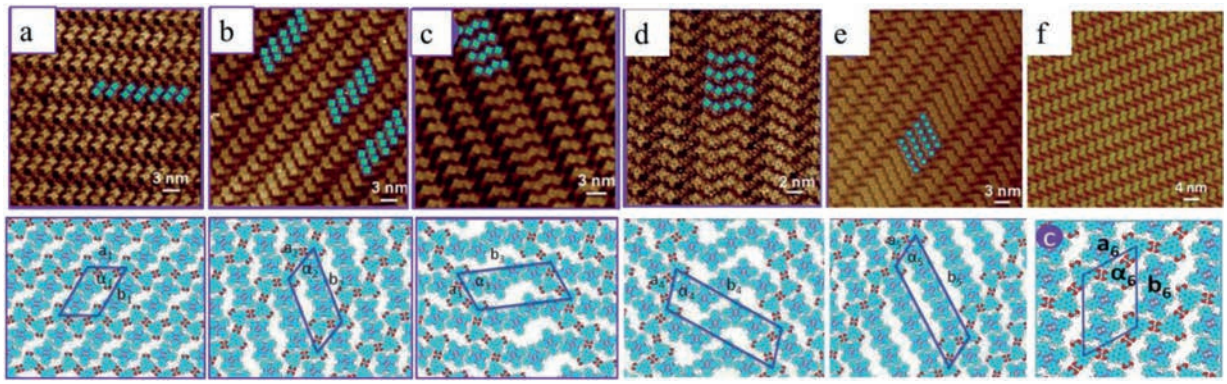

Fig. 4. An overview of the random arrays which are immobilized in the rearrangement H_3TTCA networks for the nH_2Pc@H_3TTCA system: 2H_2Pc@H_3TTCA (a), 3H_2Pc@H_3TTCA (b), 4H_2Pc@H_3TTCA (c), 5H_2Pc-zigzag@H_3TTCA (d) and 5H_2Pc-line@H_3TTCA (e), H_2Pc molecules are indicated by blue squares. (f) A high resolution STM image of the ordered the 2H_2Pc@H_3TTCA array structure after the samples were annealed. Schematic corresponding molecular models of all assemblies are presented under the STM image. Reproduced with permission [86]. Copyright 2014, The Royal Society of Chemistry.

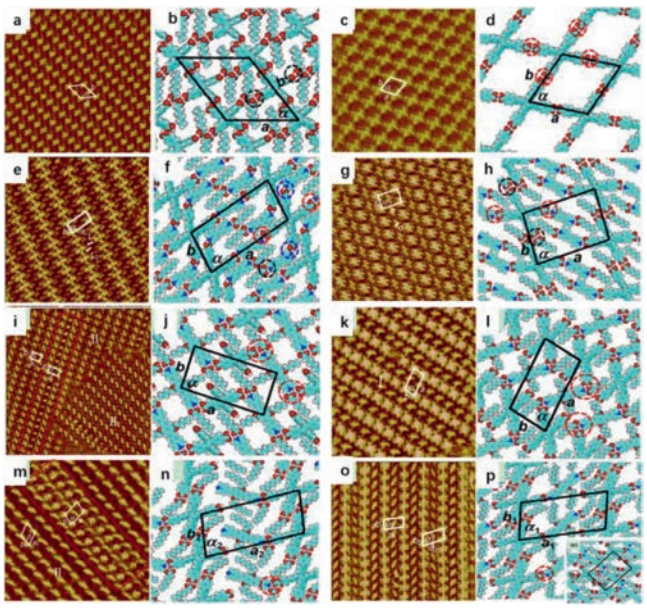

Fig. 5. High-resolution STM images of (a) H_4TCPE structure and (c) H_4ETTC structure. (b) and (d) proposed H_4TCPE and H_4ETTC self-assembled structures. High-resolution STM images of H_4ETTC/DPE structures after adding saturated DPE solution (e) and 33.33% saturated DPE solution (g). (f) and (h) Proposed molecular models of H_4ETTC/DPE structures (e) and (h) respectively. High-resolution STM images of H_4TCPE/PEBP-C4 (i) and H_4ETTC/PEBP-C4 (k). The proposed molecular models for H_4TCPE/PEBP-C4 (j) and H_4ETTC/PEBP-C4 (l). High-resolution STM images of H_4TCPE/PEBP-C8 (m) and H_4ETTC/PEBP-C8 (o). Proposed molecular model of H_4TCPE/PEBP-C8 (n) and H_4ETTC/PEBP-C8 co-assembled structures '1' and '2' (p). Reproduced with permission [95]. Copyright 2018, Tsinghua University Press and Springer-Verlag GmbH Germany.

hydrogen bonds, respectively. The H_4ETTC network structure is converted to two types of acids-pyridine-acid-pyridine structures by introducing PEBP-C8 solution. These two types of structures are classified by the orientations of PEBP-C8 molecules (Fig. 5o structures '1' and '2'). Since the self-assembly of symmetric TPE molecules could be regulated by pyridine derivatives, spatial symmetry of molecules subserves the fabrication of controllable functional structures well [95].

NNN4A is an azobenzene derivative with four carboxyl acid groups. At the HA/HOPG interface, NN4A can fabricate open Kagome networks [96], which have two types of cavities. The comparatively larger A-type cavity with sixfold symmetry is composed of six benzene rings that have hydrogen bonds between the carboxylic groups. The B-type cavity is formed from three NN4A molecules arranged in a triangular shape (Fig. 6a). The NN4A networks are considered to be a suitable molecular template for fabricating ordered guest molecule arrays. Fullerenes are highly mobile molecules and cannot self-assemble into a well-ordered array at room temperature [97]. Therefore, C_{60}, C_{80} and $Sc_3N@C_{80}$ are investigated as guest species whether can be accommodated onto the NN4A networks. The C_{60}-NN4A complex forms two kinds of assembled structures at room temperature (Fig. 6c). C_{60} molecules can be immobilized in both the A- and B-type cavities. C_{60} molecules are trapped within the A-type network as shown in Fig. 6d. The distance between the neighboring C_{60} molecules is similar to that of the NN4A network unit cell, and the space between adjacent C_{60} molecules is large enough to avoid steric C_{60}-C_{60} repulsion [98,99]. C_{60} molecules are trapped within the B-type network as observed in Fig. 6e, the distance between the adjacent C_{60} molecules is close enough that the van der Waals interaction plays a role in their stabilization in the B-type cavity [100]. C_{80} molecules have a larger diameter than C_{60} molecules. When introducing C_{80} into the NN4A cavities, C_{80} molecules only fill the A-type cavities and form well-ordered hexagonal arrays (Fig. 6h). C_{80} molecules start to show site selectivity for the two types of cavities formed by NN4A. To further analyse the inclusion selectivity of the molecular networks, $Sc_3N@C_{80}$ molecules are introduced. $Sc_3N@C_{80}$ molecules have metal atoms encapsulated within the carbon cage, which can enhance the electronic interaction between $Sc_3N@C_{80}$ molecules and the template. $Sc_3N@C_{80}$ guest molecules only occupy A-type cavities (Figs. 6k and l). The structure is essentially the same as that of C_{60} trapped in the A-type cavities but with a higher site selectivity due to the size and geometry of $Sc_3N@C_{80}$. On the basis of theoretical computations, the energy of a C_{80} or $Sc_3N@$ C_{80} molecule trapped within the A-type cavity is much larger than that trapped within the B-type cavity. Besides, the coincidence of the size and geometry of guest molecules with the A-type cavity plays a considerable role in site selectivity, thus C_{80}/NN4A and $Sc_3N@C_{80}$/NN4A A-type systems are the favorable structures. The site selection behavior of fullerenes could lead to a better comprehension of template-directed fabrication of functional molecular arrays [101].

StOF−COOH3 is a star-shaped oligofluorene derivative with three carboxylic groups. In the previous reports, StOF−COOH3 can be assembled into a cellular network with porous cavities at the octanoic acid/HOPG interface. StOF−COOH3 molecules connect with each other through hydrogen bonds between carboxylic

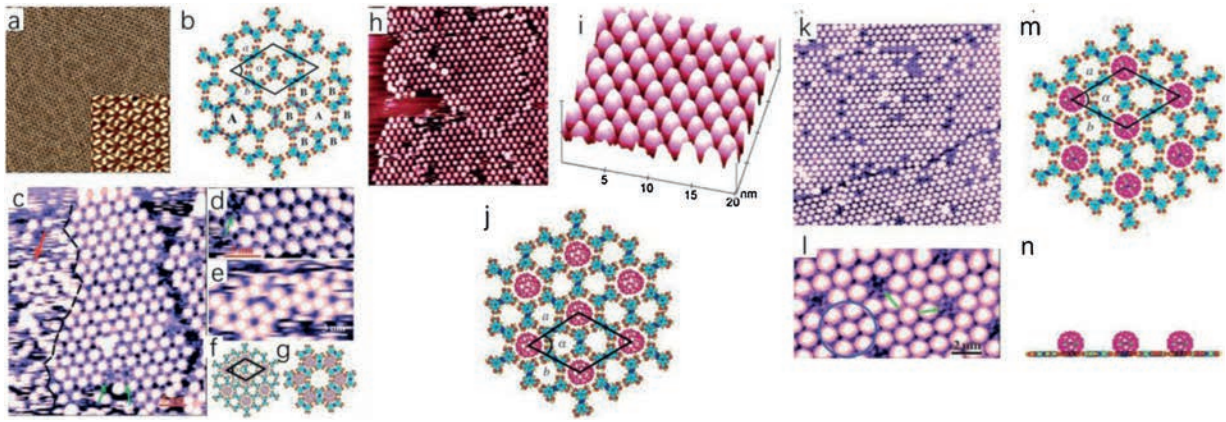

Fig. 6. (a) Constant-current STM image of a self-assembled monolayer of NN4A networks on highly ordered pyrolytic graphite (HOPG) surface. Inset: High-resolution view showing the detailed NN4A network structure. (b) Proposed molecular model for the NN4A networks. (c) Constant-current STM image of the C_{60}-NN4A host-guest architecture on an HOPG surface. (d) High-resolution view showing the detailed C_{60}-NN4A host-guest structure with C_{60} trapped within the A-type network. (e) High-resolution view showing the C_{60}-NN4A host-guest structure with C_{60} trapped within the B-type network. (f, g) Suggested molecular models of the assembled structures for (d) and (e), respectively. (h) STM image of the C_{80}-NN4A host-guest architecture on an HOPG surface. (i) High-resolution STM image of C_{80}-NN4A assembled structure. (j) Plan view of the proposed structural model. (k) STM image of the $Sc_3N@C_{80}$-NN4A host-guest architecture on an HOPG surface. (l) High-resolution STM image of the $Sc_3N@C_{80}$-NN4A structure. (m) Plan view of the proposed structural model. (n) Side view of the model. Reproduced with permission [101]. Copyright 2008, Wiley-VCH Verlag GmbH & Co. KGaA.

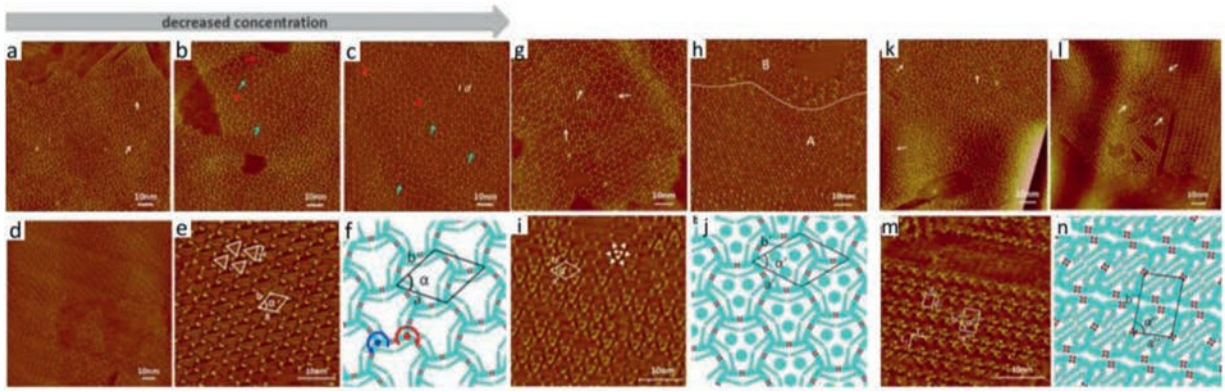

Fig. 7. Self-assembled structural transition with decreases of solvent concentration. (a) STM image of the StOF-disorder structure (undiluted). (b) STM image of the coexistence of disordered and well-ordered structure (5×dilution). (c) STM image of the StOF-honeycomb structure (5 × 5 dilution). Large scale (d) and high-resolution (e) STM image of the StOF-honeycomb structure after heating. (f) Supposed model of StOF-honeycomb network based on (e). (g) Large scale STM image of COR/StOF-honeycomb self-assembly. (h) Large-scale STM image of COR/StOF-honeycomb self-assembly after heating. (i) High-resolution STM image of COR/StOF-honeycomb self-assembly after heating. (j) Supposed molecular model based on (i). (k) STM image of COR/StOF-disorder self-assembly. (l) STM image of COR/StOF-disorder self-assembly after heating. (m) High-resolution image of StOF-ladder structure. (n) Supposed molecular model of StOF-ladder structure based on (m). Reproduced with permission [102]. Copyright 2016, American Chemical Society.

groups of neighboring StOF−COOH3. The concentration regulation of StOF−COOH3 self-assembly with solvent 1-phenyloctane has been shown in Figs. 7a-c. The StOF−COOH3 molecule achieves a self-assembly transition from a disordered structure to a honeycomb network by decreasing the concentration of StOF in the solution. After heating the honeycomb networks formed by low concentration StOF molecules, the networks will become more regular with full view of well-ordered hexagons (Figs. 7d and e). When introducing guest molecules COR into ordered honeycomb networks, triangle-shaped COR trimers are formed immediately and trapped in the triangular cavities (Fig. 7g). After a thermal annealing process, more COR trimers are formed and accommodated in the honeycomb cavities (Figs. 7h and i). When introducing COR into the disordered StOF structure (high concentration), the structure of COR trimers surrounded by six StOF molecules is observed occasionally (Fig. 7k). Altering the temperature to a higher degree like before, the disordered structure at a high StOF concentration undergoes a structural transformation of the well-ordered ladder structure (Fig. 7l). Four StOF molecules form into a rectangular cavity through hydrogen bond pairs (Fig. 7m). The cavity is completely occupied by alkyl chains of StOF−COOH3 that cannot capsulate any single COR molecule. The StOF-ladder assembly is much more stable than the honeycomb structure *via* DFT calculations [102].

Rigid disc-shaped molecule H_2TCPp is one of carboxyl-functionalized porphyrin derivatives. It is interesting that the H_2TCPp molecules can form the 2D assemblies and the bulk crystal structures. As shown in Fig. 8a, H_2TCPp molecules assemble into two types of well-ordered monolayers at the HA/HOPG interface. In structure A (Fig. 8b), the H_2TCPp molecules are aligned linearly and closely. In the line, each H_2TCPp molecule forms four pairs of hydrogen bonds through four terminal carboxyl groups to interact with two other molecules. The adjacent lines are connected with each other through van der Waals. This arrangement leads to misalignment of adjacent arrays and lack of order of structure A. While the structure B of H_2TCPp molecules is a loosely

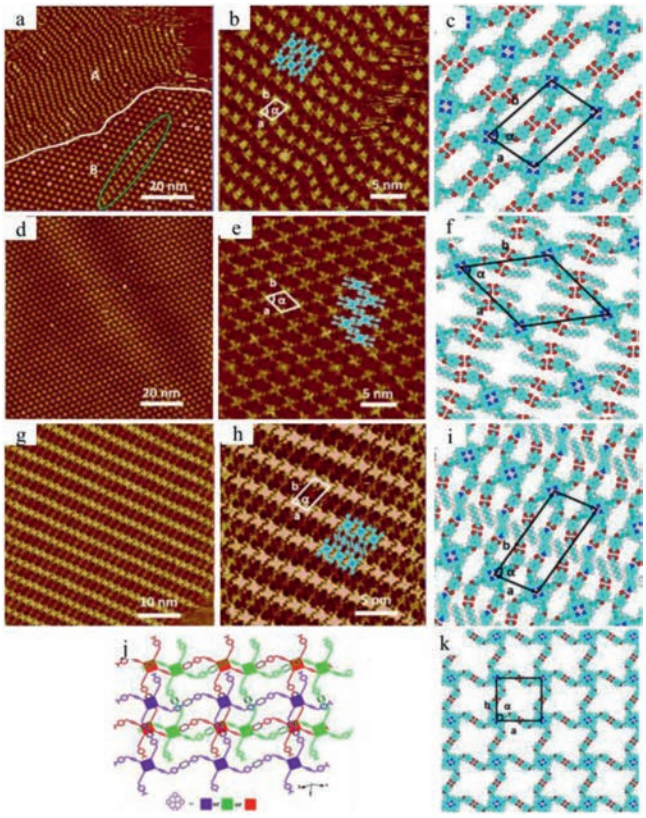

Fig. 8. (a) STM image of the self-assembled H_2TCPp molecules. (b) High-resolution STM image of structure A of H_2TCPp. Large-scale (d) and high-resolution (e) STM image of structure B of H_2TCPp. Proposed H_2TCPp molecular model of structure A (c) and structure B (f). Large-scale (g) and high-resolution (h) STM image of the co-assembled structure of H_2TCPp/DPE. (i) Proposed molecular model. (j) 3D-packing framework of H_2TCPp. (k) Proposed molecular model of structure D. Reproduced with permission [103]. Copyright 2017, American Chemical Society.

well-ordered network with large rhombus-shaped cavities (Figs. 8d and e). Four solvent molecules link to the four carboxyl groups of each H_2TCPp molecule *via* O—H···O hydrogen bonds, and the HA molecules connected with H_2TCPp interact with one another by van der Waals interaction. Introducing DPE molecules into H_2TCPp self-assembly, the H_2TCPp molecules are formed into parallel rows linked by DPE molecules *via* O—H···N hydrogen bonding and the HA molecules co-assemble with the other spare carboxyl groups of H_2TCPp molecules (Figs. 8g and h). These HA molecules interact with one another by van der Waals interactions. Compared with structure A, the width between two H_2TCPp rows of structure C is much larger and the rows are with good orderliness. Structure C is advantageous in terms of energy based on DFT calculations. The bulk crystal structures are packed up by two-dimensional monolayers by π-π packing interactions (Fig. 8j), thus the two-dimensional square geometry structure in 3D crystals is investigated for comparison with the 2D arrangements on the HOPG. In structure D, one H_2TCPp molecule is joined to other four molecules *via* H-bonding to form a square structure (Fig. 8k), which is confirmed to be unstable on the HOPG surface calculated by DFT [103].

4. Photo-isomerization on the HOPG surface

Azobenzene derivatives are a typical photochromic compound that can be reversibly isomerized from *trans* to *cis* (or *cis* to *trans*) under appropriate irradiation in solution [104]. NN4A is one of azobenzene derivatives and can form Kagome networks as shown in Fig. 9a. DPE molecules have the property of bi-pyridine mediation and photo regulation. Introducing DPE molecules into the NN4A networks, the open assemblies of NN4A are completely transformed from open Kagome networks to well-ordered rectangular networks (Fig. 9b). In the rectangular structure, two adjacent NN4A molecules in one row contact with two DPE molecules *via* N···H—O hydrogen bonds (Fig. 9d). Irradiating NN4A and DPE at UV light respectively, the DPE assembled structure cannot be obtained, while the Kagome networks of NN4A are broken and linear structures appear since the conversion of isomerism of NN4A (Fig. 9e) [105,106]. In the liner characteristics, the I-shaped *trans*-NN4A molecules become V-shaped *cis*-NN4A molecules, every *cis*-NN4A molecule is connected with four *cis*-NN4A molecules (Fig. 9f) and thus forms four pairs of hydrogen bonds. The neighboring molecules are arranged in the opposite direction from each other as distinguished in Fig. 9g. The linear structure can be reversibly converted back into the well-ordered Kagome networks after irradiation by visible light. After illuminating the UV light on the NN4A/DPE rectangular structure, the NN4A/DPE system is assembled into a zigzag structure (domain A) and a linear structure (domain B) (Fig. 9h). Linear assembly is formed by four *trans*-DPE molecules in the rectangular networks, and they are linked with one *cis*-NN4A through two pairs of N···H–O hydrogen bonds (Fig. 9j). Applying irradiation by visible light upon the zigzag structure, the rectangular network can be reformed on HOPG surface (Figs. 9k and l). The switching process of photo-isomerization of NN4A/DPE system provides a potential interest in single-molecule switch

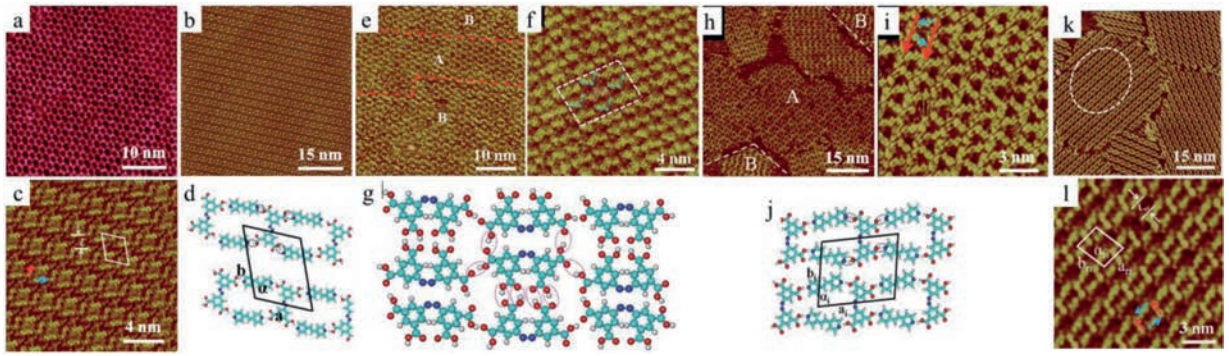

Fig. 9. (a) An STM image of the NN4A monolayer. (b) A large scale STM image of the binary structure of NN4A/DPE on the HOPG surface. (c) A high resolution STM image of the NN4A/DPE network. (d) A suggested molecular model of the NN4A/DPE network. (e) An STM image of the NN4A network after UV light irradiation, consisting of nonreacted area (domain A) and reacted area (domain B). (f) A high resolution STM image of the isomerized NN4A monolayer. (g) A suggested model of the outlined area in (f). (h) A large scale STM image of NN4A/DPE assemblies after UV light irradiation. (i) A high resolution STM image of domain A in (h). (j) A suggested model for the zigzag architecture. (k) A large scale STM image of the NN4A/DPE network by visible light irradiation after UV light irradiation. (l) A high resolution STM image of the outlined area in (k). Reproduced with permission [107]. Copyright 2012, The Royal Society of Chemistry.

fabrication by self-assembly. As the assemblies can be reversibly regulated under irradiation with UV light and visible light, the fabrication of single molecule switch by self-assembly under submolecular level shows great potential in the future [107].

5. Conclusion and prospects

In summary, we mainly discuss the molecular templates formed by the interconnection of aromatic carboxylic acids *via* hydrogen bonds, the host-guest structures which own the suitable spatial lattice of molecular templates for guest molecules, and the co-assembly with other molecules through hydrogen bonding. In these structures, hydrogen bonding plays an irreplaceable role due to its directionality and strength. The recombination of hydrogen bonds can be observed by STM, which occurs by introducing guest molecules, changing the external environment such as light, concentration, temperature, and introducing other molecules that can form hydrogen bonds.

The aromatic carboxylic acid interaction has both hydrogen bonds, van der Waals forces and π-π stacking, which is favorable for the formation of stable supramolecular structures. The carboxyl group in the aromatic carboxylic acid has a strong coordination ability and a flexible coordination mode, very advantageous for the design and construction of the molecular grid according to specific needs, thereby making it easier to design and control the structure and performance of the self-assembly. In addition, there are conjugated systems in aromatic carboxylic acids that facilitate electron transport, with potential functions in terms of light, electricity, and magnetism. Therefore, the self-assembly and regulation of aromatic carboxylic acids are of great significance and prospect.

Acknowledgments

This work was supported by the National Basic Research Program of China (No. 2016YFA0200700), and the National Natural Science Foundation of China (Nos. 21773041 and 21472029).

References

[1] V.V. Korolkov, M. Baldoni, K. Watanabe, et al., Nat. Chem. 9 (2017) 1191–1197.
[2] G. Velpula, M.M. Li, Y.B. Hu, et al., Chem.-Eur. J. 24 (2018) 12071–12077.
[3] J.Q. Li, Y.X. Qian, W.B. Duan, Q.D. Zeng, Chin. Chem. Lett. 30 (2019) 292–298.
[4] H.J. Lee, H.J. Kim, E.C. Lee, et al., Chem. -Asian J. 9 (2018) 3870–3877.
[5] S.Q. Zhang, Y.F. Geng, Y.P. Fan, et al., Phys. Chem. Chem. Phys. 19 (2017) 31284–31289.
[6] T. Fukui, S. Kawai, S. Fujinuma, et al., Nat. Chem. 9 (2017) 493–499.
[7] F. Silly, J. Phys. Chem. C 121 (2017) 10413–10418.
[8] X. Miao, L. Xu, L. Cui, W. Deng, W. Steric, Phys. Chem. Chem. Phys. 16 (2014) 12544–12553.
[9] L. Xu, X.R. Miao, L.H. Cui, et al., J. Phys. Chem. C 119 (2015) 17920–17929.
[10] B. Zha, X. Miao, P. Liu, Y. Wu, W. Deng, Chem. Commun. (Camb.) 50 (2014) 9003–9006.
[11] W. Zhang, Y. Jin, Dynamic Covalent Chemistry: Principles, Reactions, and Applications, Wiley, 2017.
[12] S. Yokoyama, T. Hirosea, K. Matsuda, Chem. Commun. (Camb.) 50 (2014) 5964–5966.
[13] Q. Bian, S. Chen, Y.M. Xing, et al., Acta Biomater. 76 (2018) 39–45.
[14] J.D. Xue, J. Xu, F.Y. Hu, et al., Phys. Chem. Chem. Phys. 16 (2014) 25765–25769.
[15] X.M. Zhang, S.D. Xu, M. Li, et al., J. Phys. Chem. C 116 (2012) 8950–8955.
[16] K. Iritani, K. Tahara, S. De Feyter, et al., Langmuir 33 (2017) 4601–4618.
[17] J.D.C. González, M. Lyoda, J.P. Rabe, Nat. Commun. 8 (2017) 14717.
[18] S. Kim, H.D. Castillo, M. Lee, et al., J. Am. Chem. Soc. 140 (2018) 4726–4735.
[19] L.Y. Zhang, J.L. Li, S.H. Qiu, X.B. Huang, Z.B. Zeng, New J. Chem. 41 (2017) 3260–3264.
[20] Z.H. Lin, C.Y. Gao, M.L. Chen, X.K. Lin, Q. He, Curr. Opin. Colloid Interface Sci. 35 (2018) 51–58.
[21] K. Cui, F. Schlutter, O. Ivasenko, et al., Chem. -Eur. J. 21 (2015) 1652–1659.
[22] W. Huang, T.Y. Zhao, M.W. Wen, et al., J. Phys. Chem. C 118 (2014) 6767–6772.
[23] K. Tahara, K. Nakatani, K. Iritani, S. De Feyter, Y. Tobe, ACS Nano 10 (2016) 2113–2120.
[24] R.K. Saravanana, I. Avasthia, R.K. Prajapatiab, et al., RSC Adv. 8 (2018) 24541–24560.
[25] R. Gatti, J.M. MacLeod, J.A. Lipton-Duffin, et al., J. Phys. Chem. C 118 (2014) 25505–25516.
[26] Y.L. Huang, W. Chen, H. Li, et al., Small 6 (2010) 70–75.
[27] E.M. Todd, S.C. Zimmerman, J. Am. Chem. Soc. 129 (2007) 14534–14535.
[28] M.Q. Dong, K. Miao, Y. Hu, et al., Phys. Chem. Chem. Phys. 19 (2017) 31113–31120.
[29] B. Wu, Y.H. Zhao, H.Y. Nan, et al., Nano Lett. 16 (2016) 3754–3759.
[30] B. van Genabeek, B.F.M. de Waal, A.R.A. Palmans, et al., Polym. Chem. 9 (2018) 2746–2758.
[31] Q.S. Stöckl, Y.C. Hsieh, A. Mairena, et al., J. Am. Chem. Soc. 138 (2016) 6111–6114.
[32] A. Ciesielski, P. Samorì, Adv. Mater. 28 (2016) 6030–6051.
[33] Q. Wei, W. Wang, E. Zhou, et al., J. Colloid Interf. Sci. 15 (2017) 58–67.
[34] M.Q. Zeng, L.X. Wang, J.X. Liu, et al., J. Am. Chem. Soc. 138 (2016) 7812–7815.
[35] M.E. Garah, A. Dianat, A. Cadeddu, et al., Small 12 (2016) 343–350.
[36] M.A. Mezour, R.M. Choueiri, O. Lukoyanova, et al., Nanoscale 8 (2016) 16955–16962.
[37] J.M. MacLeod, F. Rosei, Small 10 (2014) 1038–1049.
[38] Y. Hu, K. Miao, B. Zha, et al., Phys. Chem. Chem. Phys. 18 (2016) 624–634.
[39] F. Würthner, Acc. Chem. Res. 49 (2016) 868–876.
[40] Y. Tobe, K. Tahara, S. De Feyter, Bull. Chem. Soc. Jpn. 89 (2016) 1277–1306.
[41] S. Wieghold, J. Li, P. Simon, et al., Nat. Commun. 7 (2016) 10700.
[42] P.A. Held, H.Y. Gao, L.C. Liu, et al., Angew. Chem. Int. Ed. 55 (2016) 9777–9782.
[43] S.J. Zhan, Y. Sun, S.P. Li, et al., Polyhedron 121 (2017) 252–263.
[44] X.Y. Dong, C.D. Si, Y. Fan, et al., Cryst. Growth Des. 16 (2016) 2062–2073.
[45] C.Y. Fu, H.P. Lin, J.M. Macleod, et al., Chem. Mater. 28 (2016) 951–961.
[46] K. Miao, Y. Hu, B. Zha, et al., J. Phys. Chem. C 120 (2016) 14187–14197.
[47] H. Aitchison, H. Lu, S.W.L. Hogan, et al., Langmuir 32 (2016) 9397–9409.
[48] S. Lee, B.E. Hirsch, Y. Liu, et al., Chem. -Eur. J. 22 (2016) 560–569.
[49] A. Taraia, J.B. Baruah, Cryst. Eng. Comm. 18 (2016) 9095–9102.
[50] S. Demir, N.K. Brune, J.F. Van Humbeck, ACS Cent. Sci. 2 (2016) 253–265.
[51] A. Dasa, S. Ghosh, Chem. Commun. (Camb.) 52 (2016) 6860–6872.
[52] J.M. Hu, R. Guo, Y.G. Liu, G.H. Cui, Inorg. Chim. Acta Rev. 450 (2016) 418–425.
[53] R. Gao, D.P. Yan, Chem. Commun. (Camb.) 53 (2017) 5408–5411.
[54] S. Abb, L. Harnau, R. Gutzler, S. Rauschenbach, K. Kern, Nat. Commun. 7 (2016) 10335.
[55] W. Du, T. Wang, H.S. Chu, et al., Nature Photon. 10 (2016) 274–280.
[56] T.P. Chen, C.W. Lin, S.S. Li, et al., Adv. Energy Mater. 8 (2018)1701722.
[57] P. Gallagher, Y.L. Li, K.J. Watanabe, et al., Nano Lett. 18 (2018) 2603–2608.
[58] X. Zhang, H. Xu, Y. Shen, et al., Phys. Chem. Chem. Phys. 15 (2013) 12510–12515.
[59] Q. Yuan, Y. Xing, E. Borguet, J. Am. Chem. Soc. 132 (2010) 5054–5060.
[60] S.S. Akimenko, V.A. Gorbunov, A.V. Myshlyavtsev, Procedia Eng. 113 (2015) 108–112.
[61] J. Otsuki, Coord. Chem. Rev. 254 (2010) 2311–2341.
[62] A. Knápek, J. Sýkora, J. Chlumská, D. Sobolab, Microelectron. Eng. 173 (2017) 42–47.
[63] F. Bigourdan, J.P. Hugonin, F. Marquier, C. Sauvan, J.J. Greffet, Phys. Rev. Lett. 116 (2016)106803.
[64] B. Zha, M.Q. Dong, X.R. Miao, et al., J. Phys. Chem. Lett. 7 (2016) 3164–3170.
[65] H.Y. Gao, H. Wagner, D.Y. Zhong, et al., Angew. Chem. Int. Ed. 52 (2013) 4024–4028.
[66] B.L. Feringa, Angew. Chem. Int. Ed. 56 (2017) 11060–11078.
[67] B. Zha, X.R. Miao, P. Liu, Y.M. Wu, W.L. Deng, Chem. Commun. (Camb.) 50 (2014) 9003–9006.
[68] J. Dash, D. Trawny, J.P. Rabe, H.U. Reissig, Syn. Lett. 26 (2015) 1486–1489.
[69] A. Mairena, M. Parschau, J. Seibel, et al., Chem. Commun. (Camb.) 54 (2018) 8757–8760.
[70] H.D. Castillo, J.M. Espinosa-Duran, James R. Dobscha, et al., Chem. Commun. (Camb.) 54 (2018) 10076–10079.
[71] I. Hisaki, S. Nakagawa, N. Ikenaka, et al., J. Am. Chem. Soc. 138 (2016) 6617–6628.
[72] I. Hisaki, S. Nakagawa, N. Tohnai, M. Miyata, Angew. Chem. Int. Ed. 54 (2015) 3008–3012.
[73] H.L. Dai, S. Wang, I. Hisaki, et al., Chem. -Asian J. 12 (2017) 2558–2564.
[74] L. Peng, P. Zhu, C. Zhang, H. Xu, Prog. Chem. 25 (2013) 77–85.
[75] R.G.D. Taylor, C.G. Bezzu, M. Carta, et al., Chem. -Eur. J. 22 (2016) 2466–2472.
[76] S.Q. Zhang, R.C. Liu, L.C. Wang, et al., ACS Nano 10 (2016) 342–348.
[77] R. Zhang, L.C. Wang, M. Li, et al., Nanoscale 3 (2011) (2011) 3755–3759.
[78] L.X. Cai, L.C. Wang, S.Z. Kang, et al., J. Phys. Chem. C 120 (2016) 27259–27267.
[79] Q.Y. Zhou, Y.B. Li, Q. Li, et al., Nanoscale 6 (2014) 8387–8391.
[80] Q.N. Zeng, L. Wang, Y.W. Zhong, et al., Langmuir 30 (2014) 3034–3040.
[81] J.D. Xue, K. Deng, B. Liu, et al., RSC Adv. 5 (2015) 39291–39294.
[82] J. Xu, T. Li, Y.F. Geng, et al., J. Phys. Chem. C 119 (2015) 9227–9233.
[83] S.Q. Zhang, J.Y. Zhang, K. Deng, et al., Phys. Chem. Chem. Phys. 17 (2015) 24462–24467.
[84] M.O. Blunt, J. Adisoejoso, K. Tahara, et al., J. Am. Chem. Soc. 135 (2013) 12068-12057.
[85] K.S. Mali, M.G. Schwab, X. Feng, K. Mullen, S.D. Feyter, Phys. Chem. Chem. Phys. 15 (2013) 12495–12503.
[86] F.Y. Hu, Y.N. Gong, X.M. Zhang, et al., Nanoscale 6 (2014) 4243–4249.
[87] E.G. Zhao, Y.L. Chen, S.J. Chen, et al., Adv. Mater. 27 (2015) 4931–4937.
[88] J.B. Xiong, H.T. Feng, J.P. Sun, et al., J. Am. Chem. Soc. 138 (2016) 11469–11472.
[89] J. Shi, S. Zhang, M.M. Zheng, et al., Sensor. Actuat. B: Chem. 238 (2017) 765–771.
[90] J. Huang, N. Sun, Y.Q. Dong, et al., Adv. Funct. Mater. 23 (2013) 2329–2337.
[91] Y.L. Li, Z.P. Li, Y. Wang, Energy Environ. Sci. 6 (2013) 2907–2911.

[92] Z.J. Zhao, Z.F. Li, J.W.Y. Lam, et al., Chem. Commun. (Camb.) 47 (2011) 6924–6926.
[93] Z.J. Zhao, T.X. Chen, S.T. Jiang, et al., J. Mater. Chem. C Mater. Opt. Electron. Devices 4 (2016) 4800–4804.
[94] Z.G. Chi, X.Q. Zhang, B.J. Xu, et al., Chem. Soc. Rev. 41 (2012) 3878–3896.
[95] X. Peng, L.X. Cheng, X.Y. Zhu, et al., Nano Res. 11 (2018) 5823–5834.
[96] S. Furukawa, H. Uji-i, K. Tahara, et al., J. Am. Chem. Soc. 128 (2006) 3502–3503.
[97] H. Zhou, H. Dang, J.H. Yi, et al., J. Am. Chem. Soc. 129 (2007) 13774–13775.
[98] B. Xu, C.G. Tao, W.G. Cullen, J.E. Reutt-Robey, E.D. Williams, Nano Lett. 5 (2005) 2207–2211.
[99] G.B. Pan, X.H. Cheng, S. Hoger, W. Freyland, J. Am. Chem. Soc. 128 (2006) 4218–4219.
[100] E. Mena-Osteritz, P. BOuerle, Adv. Mater. 18 (2006) 447–452.
[101] M. Li, K. Deng, S.B. Lei, et al., Angew. Chem. Int. Ed. 47 (2008) 6717–6721.
[102] H.L. Dai, W.J. Yi, K. Deng, H. Wang, Q.D. Zeng, ACS Appl. Mater. Interfaces 8 (2016) 21095–21100.
[103] J.F. Hou, H.L. Dai, Z.Q. Zhang, et al., Langmuir 33 (2017) 400–406.
[104] A. Natansohn, P. Rochon, Chem. Rev. 102 (2002) 4139–4175.
[105] Y.T. Shen, K. Deng, X.M. Zhang, et al., Nano Lett. 11 (2011) 3245–3250.
[106] D. Bleger, A. Clesielki, P. Samori, S. Hecht, Chem. Eur. J. 16 (2010) 14256.
[107] X.M. Zhang, S. Wang, Y.T. Shen, et al., Nanoscale 4 (2012) 5039–5042.